Article

Discovery Medicine 2025; 37(199): 1534–1547
https://doi.org/10.24976/Discov.Med.202537199.133

Unveiling Key cGAS–STING Pathway-Related Molecular Players in Arteriosclerosis Development: A Comprehensive Bioinformatics Analysis

Fuzhen Zheng[1,†], Licheng Yan[1,†], Yuanxiang Chen[1], Deng Xie[1], Feng Zhu[2,*], Guoxing Weng[1,*]

[1]Department of Cardiovascular Surgery, Shengli Clinical Medical College of Fujian Medical University, Fujian Provincial Hospital, 350001 Fuzhou, Fujian, China
[2]Department of Vascular Surgery, General Surgery Clinical Center, Shanghai General Hospital, Shanghai Jiao Tong University School of Medicine, 201613 Shanghai, China
*Correspondence: zf1102866281@163.com (Feng Zhu); wengguoxing@fjmu.edu.cn (Guoxing Weng)
†These authors contributed equally.
Published: 20 August 2025

Background: Arteriosclerosis (AS) is a globally prevalent disease for which there is currently no effective treatment. Therefore, identifying potential drug targets is of crucial importance. The Cyclic guanosine monophosphate–adenosine monophosphate synthase (cGAS)–STING pathway is an intracellular immune sensing mechanism that detects DNA damage and viral infections, and it could contribute to the progression of AS through its influence on immune regulation. By using bioinformatics methods, we identified critical genes involved in the progression of AS that are associated with the cGAS–STING pathway, providing potential molecular targets for further investigation.

Methods: Datasets related to AS were extracted from the Gene Expression Omnibus (GEO) database, including GSE100927, GSE28829, and GSE43292. Furthermore, we conducted a search in the GeneCards database to identify genes associated with the cGAS–STING signaling pathway. Key gene identification was carried out through comparative expression analysis using Limma and weighted gene co-expression network analysis (WGCNA). Machine learning (ML) algorithms were then applied to screen and evaluate the diagnostic value of potential biomarkers. After obtaining both cGAS–STING-related and AS-related differentially expressed genes (cASDEGs), we utilized gene set enrichment analysis (GSEA) approach to analyze the potential function of cASDEGs and CIBERSORT algorithm to assess immune cell infiltration in AS. Finally, experiments including reverse transcription quantitative polymerase chain reaction (RT-qPCR), Western blotting and immunofluorescence were conducted to validate the expression patterns of cASDEGs.

Results: By intersecting the Limma and WGCNA results, we identified a total of 741 differentially expressed genes (DEGs) related to AS from the GSE100927 dataset. An intersection of these DEGs with the cGAS–STING-related genes identified 16 cASDEGs. Four pivotal cASDEGs (C-src tyrosine kinase (*CSK*), fatty acid binding protein 5 (*FABP5*), B-cell lymphoma 2-associated athanogene (*BAG2*), and alpha-galactosidase A (*GLA*)) were identified through the ML-based screening, all of which showing significant diagnostic relevance. Further immune profiling uncovered dysregulated immunity in AS and a link between these genes and immune cell interactions. Experimental validation confirmed that the four central cASDEGs exhibited expression patterns aligning with the bioinformatics predictions.

Conclusion: Our study identified four genes (*CSK*, *FABP5*, *BAG2*, and *GLA*) that may promote the development of AS through the cGAS–STING pathway, providing new insights into the pathogenesis and potential treatment of AS.

Keywords: Arteriosclerosis; cGAS–STING; bioinformatics analysis; machine learning; immune cell infiltration

Introduction

With increasing annual incidence rate, cardiovascular diseases are among the leading causes of mortality in humans, posing substantial health risk to affected individuals and hindering social development [1,2]. Arteriosclerosis (AS) serves as the common pathological denominator for various cardiovascular pathologies, encompassing coronary heart disease, cerebral infarction, and extremity arterial diseases [3,4]. AS is a slow-progressing, chronic disease of large- and medium-sized arteries, mainly characterized by plaque formation on the inner arterial walls [5]. The intimal layer beneath the vascular endothelium undergoes pathological changes characterized by the accumulation and transformation of lipids, cholesterol, calcium, thrombi, inflammatory cells, smooth muscle cells, and

necrotic debris within atherosclerotic plaques [6], which is a prolonged process involving various pathological stages. Nevertheless, the underlying causes and molecular mechanisms remain elusive, warranting in-depth investigation of AS pathogenesis and treatments for improving physical, mental, and social health.

Mitochondrial dysfunction is closely related to the onset, progression, and cell death in AS. Excessive reactive oxygen species levels can damage cellular macromolecules such as DNA, lipids, and proteins, inducing cell death pathways such as cell necrosis, apoptosis, autophagy, and ferroptosis, thereby promoting AS plaque formation [7,8]. Cyclic guanosine monophosphate–adenosine monophosphate synthase (cGAS) is a cytoplasmic DNA recognition receptor that can recognize exogenous DNA (such as viral and bacterial DNA), the host DNA (such as mitochondrial DNA [mtDNA] and nuclear DNA) and damaged DNA [9], thereby activating the cGAS–STING signaling pathway and initiating the innate immune response [10]. Reportedly, the cGAS–STING signaling pathway plays an important role in tumors, autoimmune diseases, and chronic inflammatory conditions [11]. Recent evidence also suggests that mitochondrial dysfunction–mediated oxidative stress and cytoplasmic release of mtDNA can activate the cGAS–STING signaling pathway. While this pathway is predominantly active in immune cells, it is also expressed in endothelial and epithelial cells [12]. Notably, cGAS–STING activation in vascular smooth muscle cells has been shown to contribute to their phenotypic switching [13], and its activation in endothelial cells regulates cell proliferation and inflammatory responses. These findings provide a rationale for investigating the cGAS–STING signaling pathway in the context of AS, although its role in AS remains incompletely defined. To elucidate the function of cGAS–STING signaling in AS pathophysiology, bioinformatics analysis offers a novel complementary approach to experimental validation, providing a more in-depth and holistic method to unravel the disease's pathogenesis.

This study aimed to identify critical genes involved in the cGAS–STING pathway that could serve as potential molecular targets for treating AS. In this study, we employed a bioinformatics-driven approach to analyze publicly available AS-related datasets. Differential expression analysis, weighted gene co-expression network analysis (WGCNA), and machine learning (ML) techniques were integrated to identify potential therapeutic targets with strong diagnostic potential. Furthermore, *in vitro* validation of the bioinformatics findings was conducted using reverse transcription quantitative polymerase chain reaction (RT-qPCR), Western blotting, and immunofluorescence.

Materials and Methods

Research Design and Data Source

The study design is illustrated in Fig. 1. Herein, three AS-related datasets were retrieved from the National Center for Biotechnology Information Gene Expression Omnibus database (https://www.ncbi.nlm.nih.gov/geo/) [14], namely GSE100927, GSE43292, and GSE28829. GSE100927 is based on the GPL17077 platform and includes 35 control arteries from organ donors and 69 peripheral arteries from individuals with AS, including carotid, femoral, and popliteal arteries. GSE43292 is based on the GPL6244 platform and consists of 32 carotid artery samples, each for the non-AS and AS groups. GSE28829 is based on the GPL570 platform and comprises 13 patients with early pathological intimal thickening of the carotid artery and 16 patients with late fibrous-cap atherosclerotic carotid artery plaque. GSE100927 was used as the training set owing to its substantial sample size, and GSE43292 and GSE28829 served as external validation sets for ML. Detailed information regarding the datasets can be found in **Supplementary Table 1**.

Data Processing and Screening for Differentially Expressed Genes

The significant differentially expressed genes (DEGs) in GSE100927 were identified using the R software (R Foundation for Statistical Computing, Vienna, Austria) version 4.3.1 package "limma version 3.56.2". The dataset was normalized using the normalizeBetweenArrays function. After normalization, a linear model was fitted using lmFit, and contrasts were defined with makeContrasts. The eBayes method was employed for statistical testing with eBayes. Differential expression was determined based on an absolute log fold change exceeding 0.585 and a false discovery rate–adjusted p-value below 0.05. To visualize the DEGs, we generated a heatmap using the "pheatmap version 1.0.12" and "ggplot2 version 3.4.3" R software packages [15].

Weighted Gene Co-Expression Network Construction and Gene Module Identification

The WGCNA R package version 1.72-5 was applied to construct co-expression networks and identify gene modules [16]. After standardizing the expression matrix, genes within the top 25% variance were selected for module construction. We used the goodSamplesGenes function to screen for and remove outliers. Sample clustering and trait heatmap were generated using hierarchical clustering. The pickSoftThreshold function was applied to identify the optimal soft-thresholding power for network construction. Using this value, an adjacency matrix was generated and further converted into a topological overlap matrix (TOM). Next, hierarchical clustering was performed using TOM-differential measurement, with a minimum module size of

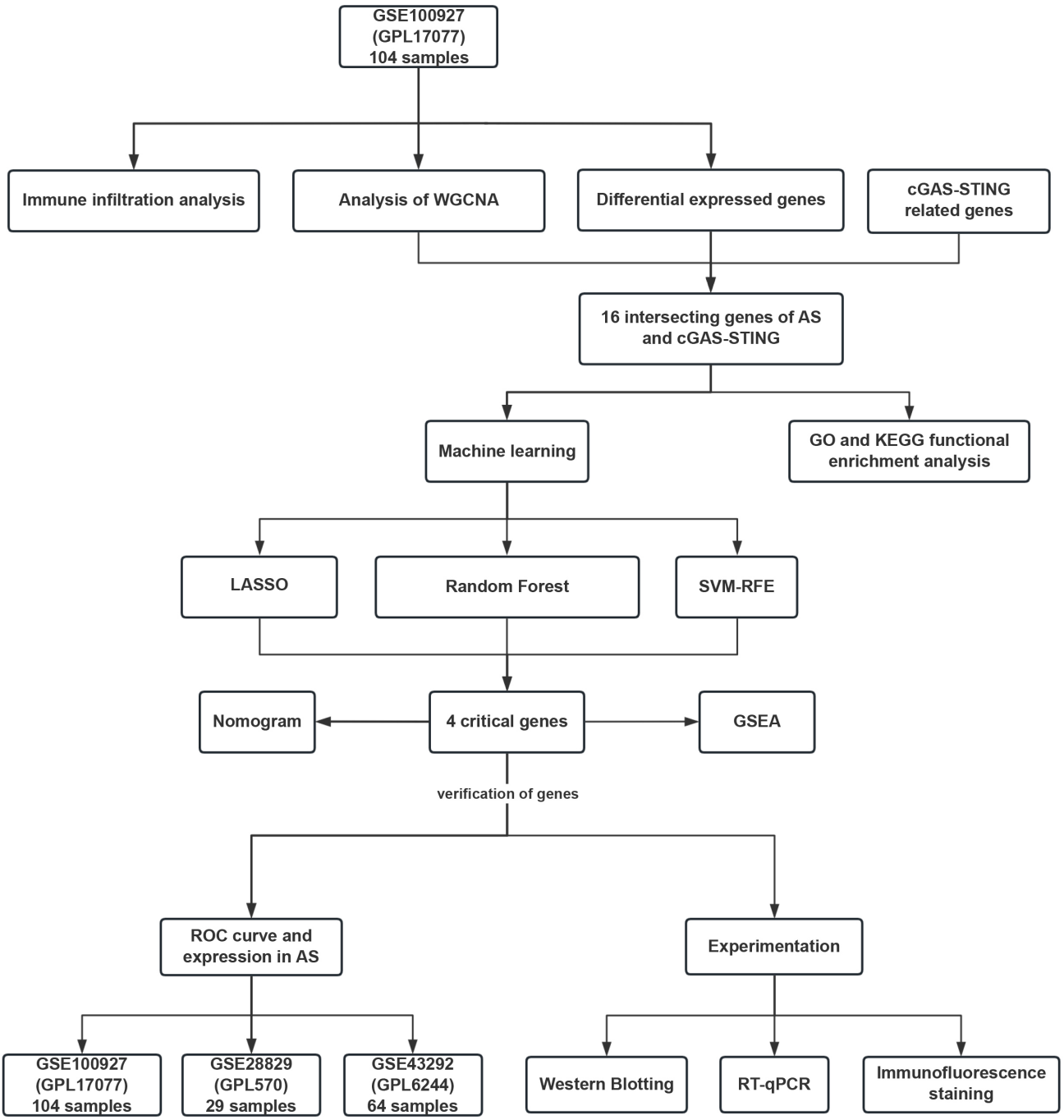

Fig. 1. Flow chart depicting the study design. Abbreviations: AS, Arteriosclerosis; cGAS, Cyclic guanosine monophosphate–adenosine monophosphate synthase; DEGs, differentially expressed genes; GO, Gene Ontology; GSEA, gene set enrichment analysis; KEGG, Kyoto Encyclopedia of Genes and Genomes; LASSO, Least Absolute Shrinkage and Selection Operator; RT-qPCR, reverse transcription quantitative polymerase chain reaction; ROC, receiver operating characteristic; SVM-RFE, support vector machine recursive feature elimination; WGCNA, weighted gene co-expression network analysis.

150, to obtain gene modules. Random colors were assigned to each module. Dynamic tree cutting was performed to identify modules, and module eigengenes were calculated. Module-trait relationships were explored, and module membership (MM) and gene significance (GS) were computed. We generated scatter plots for MM *vs.* GS and identified hub genes within each module. Following this, the module most closely related to AS was selected. Specifically, genes with a module membership of >0.8 and a gene significance of >0.5 were selected as core AS-related genes for further analysis.

AS-Related Differentially Genes Identification and Functional Enrichment Analysis

AS-related DEGs were identified by intersecting the AS-related genes obtained from WGCNA with the DEGs identified using the "limma" software package. The candidate genes underwent functional characterization employing the 'org.Hs.eg.db' (v3.17.0) annotation database. To elucidate the biological significance of AS-associated DEGs, we implemented comprehensive Gene Ontology (GO) and Kyoto Encyclopedia of Genes and Genomes (KEGG) pathway enrichment analyses using 'clusterProfiler' (v4.8.3) [17], examining biological processes, cellular components, and molecular functions domains. Statistical significance was determined at $p < 0.05$.

Identification Both cGAS–STING-Related and AS-Related Differentially Genes (cASDEGs)

In the GeneCards database, the keyword "cGAS–STING", with a cutoff date of 1 May 2024, was searched, yielding 435 genes (**Supplementary Table 2**). These cGAS–STING-related genes were intersected with AS-related DEGs, leading to the identification of 16 cASDEGs.

Machine Learning Screening of Critical cASDEGs

This investigation employed a tripartite ML approach, utilizing Least Absolute Shrinkage and Selection Operator (LASSO) regression, support vector machine (SVM) classification, and random forest (RF) ensemble learning to pinpoint critical cASDEGs. For the LASSO logistic regression model, coefficients of non-contributory variables were reduced to zero, allowing for the selection of the most relevant genes. The SVM framework, which is a supervised ML technique, was used for binary classification. It maximizes the classification margin by identifying the optimal model without relying on sample size. In contrast, RF analysis is an ensemble learning method based on decision trees, with a focus on individual variable scores. The "glmnet version 4.1-8" package [18] was utilized for LASSO regression, while the "e1071 version 1.7-14" [19] and "caret version 6.0-94" [20] packages were used for SVM analysis. For RF analysis, the "randomForest version 4.7-1.1" package [21] was employed. To obtain the optimal λ for LASSO regression, repeated 10-fold cross-validation resampling iterations were performed. The performance of the SVM and RF models was assessed using 10-fold cross-validation, with a consistent random seed applied across all three methods [22]. Finally, genes that were identified as overlapping in the results obtained from the LASSO, SVM, and RF analyses were considered potential critical cASDEGs.

Receiver Operating Characteristic Curve Verification and Nomogram Construction

The clinical values of the critical cASDEGs in AS progression were assessed using the three retrieved datasets: GSE100927 for internal validation; GSE43292 and GSE28829 for external validation. The diagnostic performance was assessed by generating receiver operating characteristic (ROC) curves with the "pROC version 1.18.5" package in R, and the corresponding area under the curve (AUC) values were computed. Genes with AUC values of >0.75 were considered to exhibit notable diagnostic value. The nomogram calibration curves were internally validated using the GSE100927 dataset to assess the agreement between predicted probabilities and actual observed outcomes. Calibration plots were generated to visually evaluate the performance of the nomogram, ensuring its reliability in predicting disease progression. A diagnostic curve plot was generated using the R software package "rma version 3.0".

Immunocyte Infiltration Measurement, Evaluation, and Correlation Analysis

The GSE100927 dataset was used to analyze immunocyte infiltration. The infiltration levels of 22 immune cell types were evaluated using the "CIBERSORT" package [23] with the "LM22" file (https://cibersortx.stanford.edu/). Following this, the results were screened based on the $p < 0.05$. Bar graphs were used to visualize the differences in the levels of the 22 infiltrating immune cell types between the AS and non-AS groups, and box plots were used for intergroup comparisons. Heatmaps were generated to depict the correlation between cASDEGs and immune cells. R software packages such as "ggpubr version 0.6.0", "vioplot version 0.4.0", "corrplot version 0.92", and "ggplot2 version 3.4.4" were used for visualization.

GSEA Enrichment Analysis

To examine variations in enriched biological pathways between subgroups, we conducted GSEA employing the clusterProfiler (v4.8.3). The disease cohort was stratified into two subgroups according to median expression levels of the core coronary artery sclerosis-associated DEGs, enabling comparison of pathway enrichment patterns between high- and low-expression populations. Mean expression levels for each group were calculated, with extremely low values adjusted to a small positive constant to prevent logarithmic errors. The log fold change (logFC) between groups was computed and ranked in descending order to prepare the dataset for GSEA. The analysis utilized the "c2.cp.kegg.symbols" gene set from the MSigDB database (https://www.gsea-msigdb.org/gsea/).

Sample Collection

The samples were collected from patients undergoing femoral arterial–femoral artery bypass in the Fujian Provincial Hospital ($n = 5$). Atherosclerotic blood vessel samples were obtained from the lesion area and normal blood vessels were obtained from the bypass area. The specimens were stored in liquid nitrogen at –80 °C within 1 hour of collection for long-term preservation. This study was approved

by the Ethics Committee of our hospital (license number: K2021-04-042). Informed consent was obtained from all participants. The comprehensive clinical data of all patients is presented in **Supplementary Table 3**.

RT-qPCR

Total RNA was extracted from tissue samples using TRIzol reagent (Invitrogen, Carlsbad, CA, USA), followed by quantification of RNA quality and yield using a Nanodrop 2000 spectrophotometric system (Thermo Fisher Scientific, Waltham, MA, USA). Subsequent complementary DNA synthesis was carried out with 500 ng RNA input according to standard procedures. Reverse transcription quantitative polymerase chain reaction (RT-qPCR) was conducted on a CFX96 Touch system (Bio-Rad, Hercules, CA, USA) using iTaq Universal SYBR Green (Bio-Rad, Hercules, CA, USA). Gene expression levels were calculated using the $2^{-\Delta\Delta Ct}$ method, with β-actin as the internal reference. Primer sequences are provided in **Supplementary Table 4**.

Western Blotting

Tissue samples were lysed on ice using radioimmunoprecipitation assay (RIPA) buffer (KGB5203, KeyGEN BioTECH, Nanjing, China) to extract proteins. Twenty micrograms of protein were separated by sodium dodecyl sulfate–polyacrylamide gel electrophoresis (SDS-PAGE) and transferred onto a polyvinylidene fluoride (PVDF) membrane (FFP22, Beyotime, Shanghai, China). The membrane was then blocked with Tris-buffered saline with Tween 20 (TBST) containing 5% non-fat milk for 2 hours at room temperature. Subsequently, the blocked membrane was incubated overnight at 4 °C with primary antibodies targeting C-src tyrosine kinase (CSK; 1:1000; 17720-1-AP; Proteintech, Wuhan, China), fatty acid binding protein 5 (FABP5; 1:1000; 12348-1-AP; Proteintech, Wuhan, China), B-cell lymphoma 2-associated athanogene (BAG2; 1:1000; 29820-1-AP; Proteintech, Wuhan, China), alpha-galactosidase A (GLA; 1:1000; 66121-1-Ig; Proteintech, Wuhan, China), and β-actin (1:20,000; 66009-1-Ig; Proteintech, Wuhan, China). After three washes with TBST, the membrane was incubated at room temperature for 1 hour with horseradish peroxidase (HRP)-conjugated secondary antibodies (1:2000; AT0097 and AT0098, Engibody, Shanghai, China). Protein bands exhibiting immunoreactivity were detected through enhanced chemiluminescence (ECL) methodology (P0018S, Beyotime, Shanghai, China), with subsequent digital documentation performed using a computerized gel imaging apparatus.

Immunofluorescence Staining

The collected samples were fixed in 4% paraformaldehyde (P0099, Beyotime, Shanghai, China) for 24 hours, then dehydrated, embedded in paraffin, and sectioned into 4 µm thick slices for immunofluorescence staining. The sections were dewaxed and rehydrated, followed by antigen retrieval using 10 mM sodium citrate buffer (pH 6.0) heated in a microwave at high temperature for 5–10 minutes. They were then permeabilized with 0.1% Triton X-100 (ST797, Beyotime, Shanghai, China), blocked with 5% bovine serum (ST2254, Beyotime, Shanghai, China), and incubated overnight at 4 °C with primary antibodies against CSK (1:200; 17720-1-AP; Proteintech, Wuhan, China), FABP5 (1:200; 12348-1-AP; Proteintech, Wuhan, China), BAG2 (1:200; ab229089; Abcam, Cambridge, MA, USA), and GLA (1:200; 66121-1-Ig; Proteintech, Wuhan, China). The secondary antibody (1:400, A23410 or A23420, Abbkine, Wuhan, China) was applied for 1 hour at room temperature away from the light. Nuclei were stained with DAPI (C1005, Beyotime, Shanghai, China), and after the final wash, the slides were mounted with 50% glycerol. The sections were then visualized using a fluorescence microscope (Olympus, Tokyo, Japan).

Data Analysis Methods

Statistical analyses were performed to analyze the results of wet experiments and assess the differences in the baseline data among included patients. The data are presented as mean ± standard deviation for independent experiments. Differential analyses were performed using Student's *t*-tests with the Statistical Package for the Social Sciences (SPSS) version 26.0 (IBM Corp., Armonk, NY, USA). GraphPad Prism was used for statistical graph drawing (version 9.0, GraphPad Software Inc., San Diego, CA, USA). $p < 0.05$ was considered statistically significant.

Results

Identification of DEGs and AS-Related Genes

From the GSE100927 dataset, a total of 1656 DEGs were obtained, consisting of 990 upregulated and 666 downregulated genes (volcano plot, Fig. 2A; heatmap, Fig. 2B; **Supplementary Table 5**). The top 25% of genes with the highest variance were selected for further analysis. Utilizing the appropriate soft threshold parameter ($\beta = 10$) and a scale R^2 value of 0.83, a scale-free network was constructed (**Supplementary Fig. 1A,B**), and seven significant modules were identified (TOM heatmap, Fig. 2C,D; **Supplementary Fig. 1C**). Among them, the turquoise module exhibited a strong association with AS (Fig. 2E), presenting 1162 AS-related genes based on the criteria of module membership >0.8 and gene significance >0.5 (Fig. 2F, **Supplementary Table 6**).

AS-Related DEGs Identification and Functional Enrichment Analysis

The intersection of DEGs identified by the limma package and AS-related genes revealed 741 genes as AS-related DEGs (Fig. 3A, **Supplementary Table 7**). Gene Ontology (GO) analysis showed that in both disease and

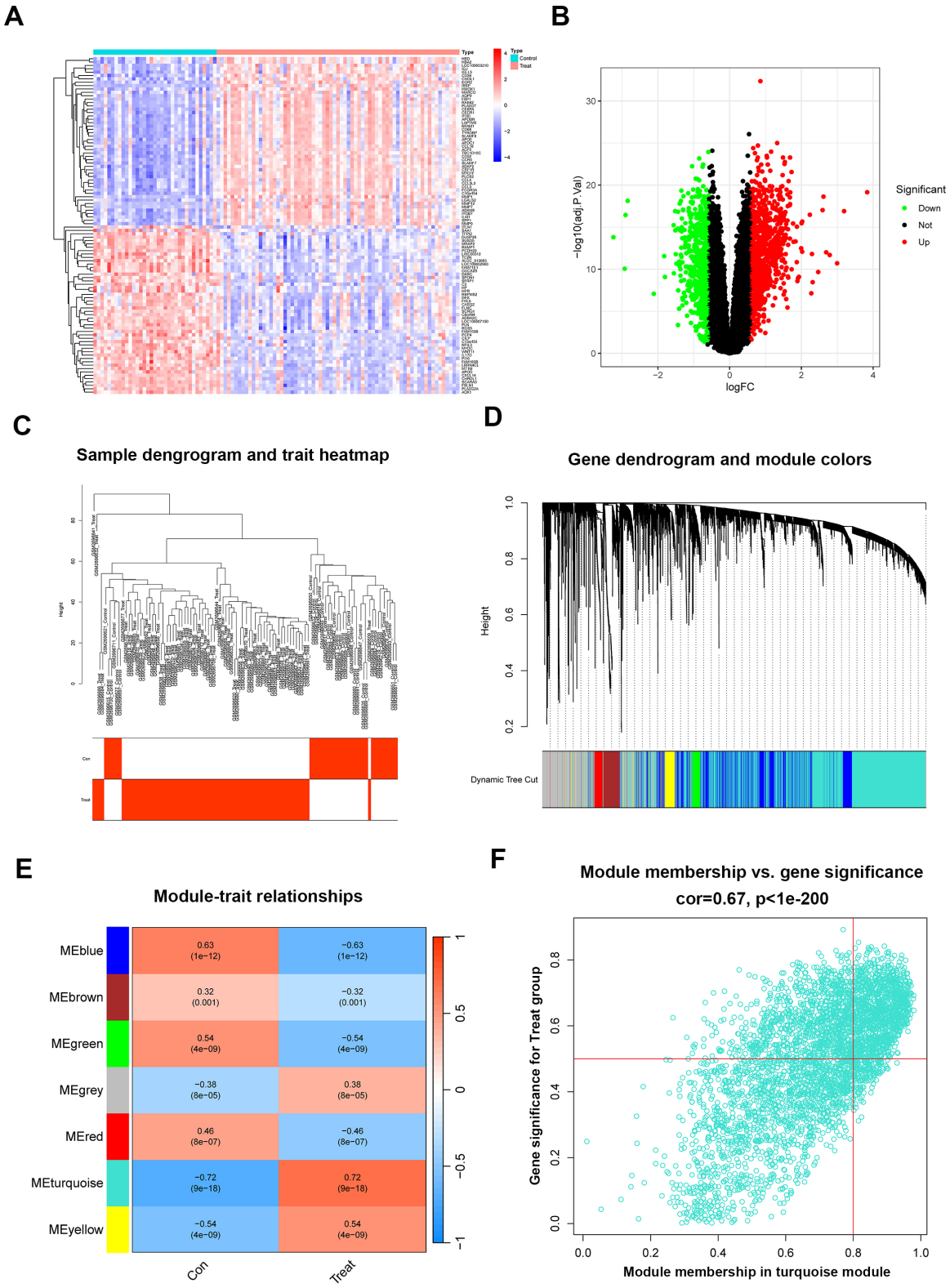

Fig. 2. Expression analysis of DEGs and weighted co-expression network construction based on the GSE100927 dataset. (A) Heatmap showing the top 50 DEGs. (B) Volcano plot of DEGs. (C) Sample clustering dendrogram with trait heatmap. (D) Cluster dendrogram illustrating co-expression modules. (E) Correlation analysis of eigengene-clinical status relationships in control versus AS populations. (F) Scatter plot illustrating turquoise module gene participation versus AS biological relevance. Abbreviations: AS, Arteriosclerosis; DEGs, differentially expressed genes.

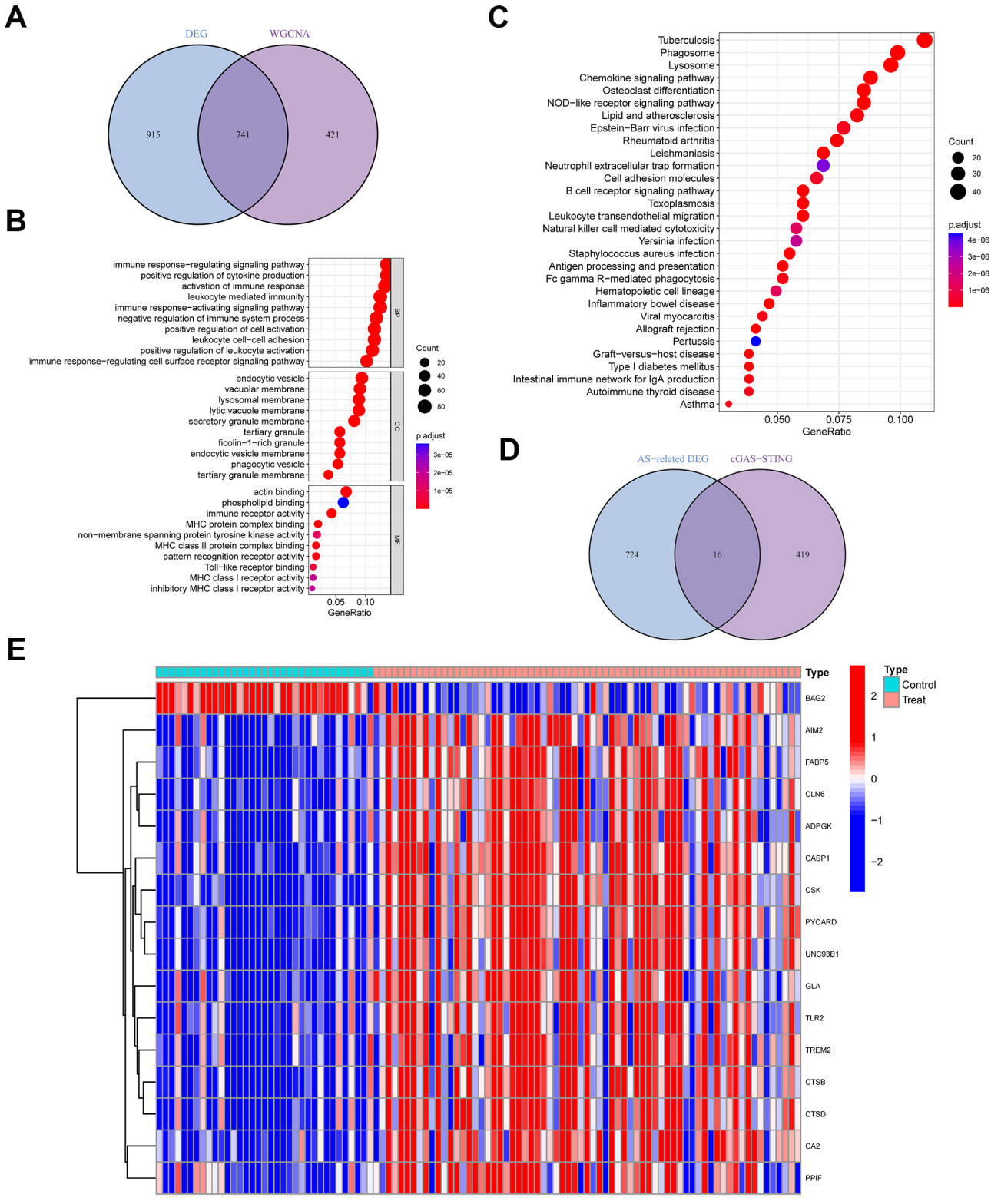

Fig. 3. Functional enrichment analysis of AS-related DEGs and the selection of cGAS–STING and AS-related DEGs (cASDEGs). (A) Identification of AS-related DEGs. (B) Heatmap of the cASDEGs in GSE100927. (C) Identification of cASDEGs. (D) GO enrichment of AS-related DEGs. (E) KEGG enrichment of AS-related DEGs. Abbreviations: AS, Arteriosclerosis; DEGs, differentially expressed genes; GO, Gene Ontology; KEGG, Kyoto Encyclopedia of Genes and Genomes.

control samples (Fig. 3B, **Supplementary Table 8**), DEGs were predominantly enriched in biological processes such as immune response-regulating signaling pathways, positive regulation of cytokine production, and immune activa-

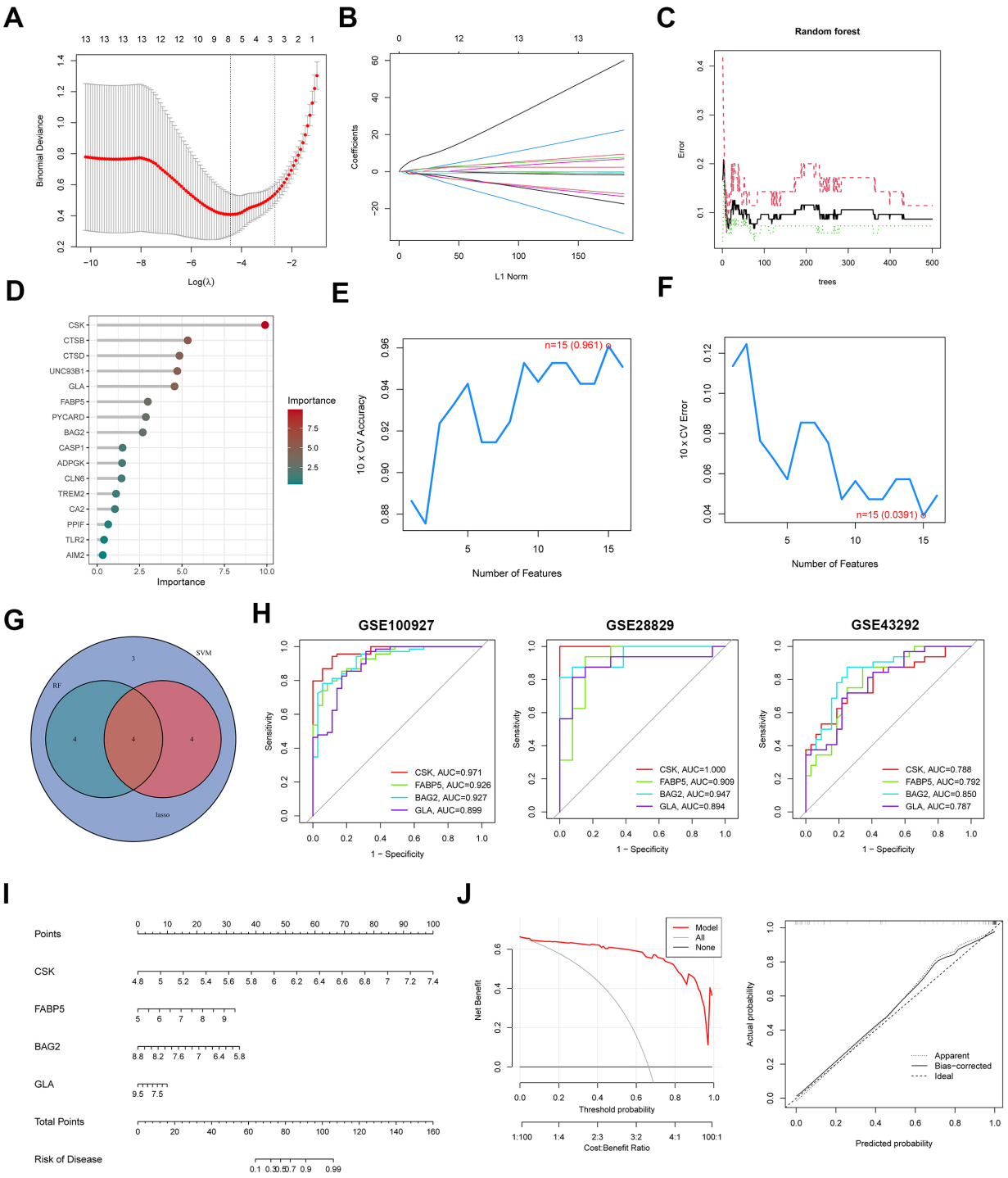

Fig. 4. Core cASDEGs selection by machine learning and verification. (A,B) Eight genes were identified through the LASSO regression algorithm. (C,D) Random forest algorithm selected eight genes. (E,F) The SVM-RFE algorithm was used to extract 15 genes. (G) Identification of the four core cASDEGs based on three machine learning results (*CSK*, *FABP5*, *BAG2*, and *GLA*). (H) ROC curve of the four core cASDEGs in the GSE100927 (left panel), GSE28829 (middle panel), GSE43292 (right panel). (I) Construction of a nomogram for predicting the risk of AS based on the four core cASDEGs. (J) The calibration curve and the decision curve analysis of nomogram. Abbreviations: AS, Arteriosclerosis; cASDEGs, cGAS–STING-related and AS-related differentially expressed genes; LASSO, Least Absolute Shrinkage and Selection Operator; ROC, receiver operating characteristic; SVM-RFE, support vector machine recursive feature elimination; *CSK*, C-src tyrosine kinase; *FABP5*, fatty acid binding protein 5; *BAG2*, B-cell lymphoma 2-associated athanogene; *GLA*, alpha-galactosidase A.

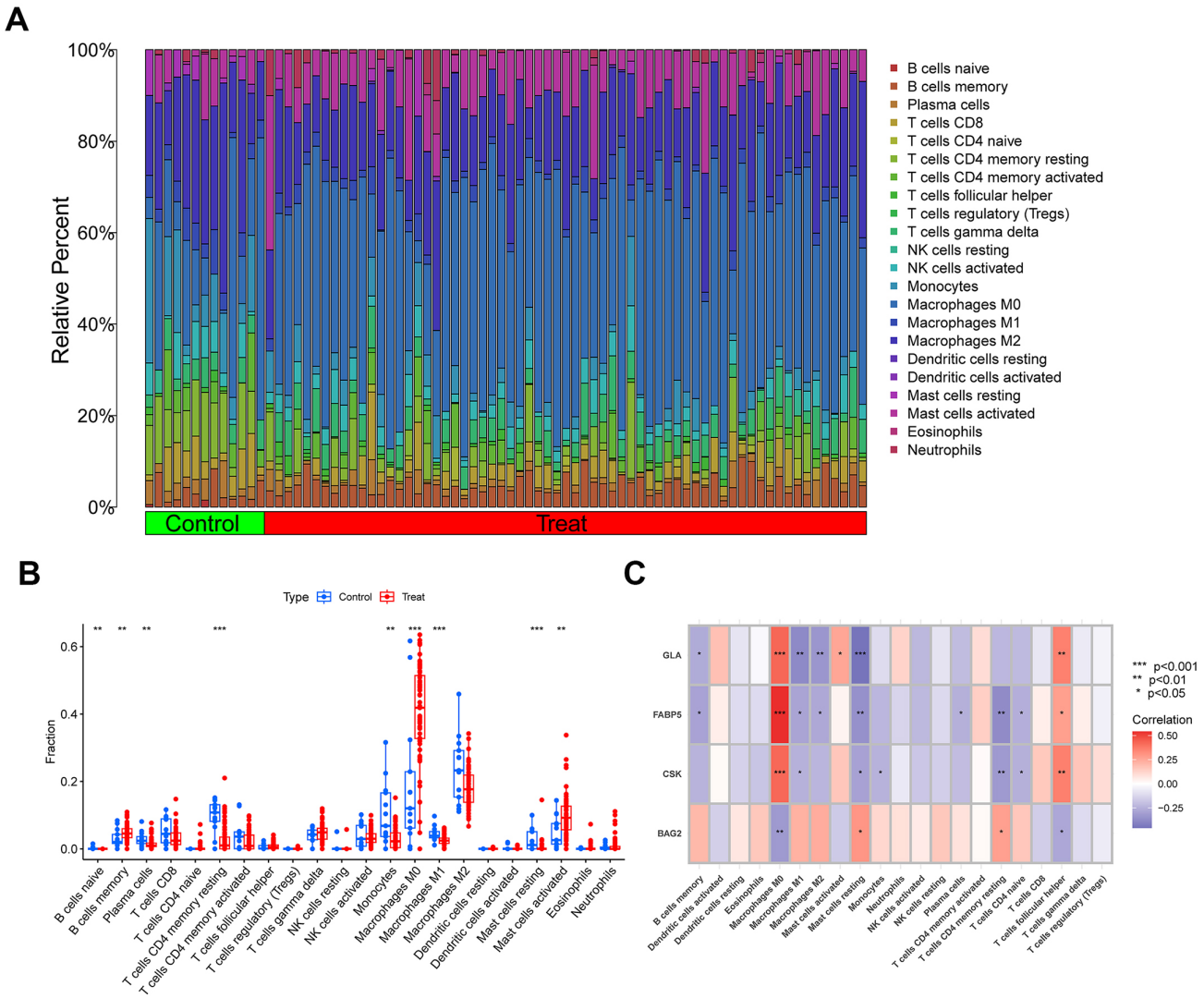

Fig. 5. Immune cell infiltration profiling in AS patients. (A) A bar graph illustrating the relative distribution of 22 types of immune cells in AS and control samples. (B) Boxplots displaying differences in immune cell infiltration levels between AS patients and healthy controls. (C) Correlation patterns between the four key cASDEGs and the abundance of infiltrating immune cells. *$p < 0.05$, **$p < 0.01$, ***$p < 0.001$ (the Control group *vs.* the Treat group). Abbreviations: AS, Arteriosclerosis; cASDEGs, cGAS–STING-related and AS-related differentially expressed genes.

tion; cellular components including endocytic vesicles, vacuolar membranes, and lysosomal membranes; and molecular functions like actin binding, phospholipid binding, and immune receptor activity. The Kyoto Encyclopedia of Genes and Genomes (KEGG) pathway analysis revealed enrichment in pathways related to osteoclast differentiation, lipids, and AS (Fig. 3C, **Supplementary Table 9**).

Identification of Critical cASDEGs Through ML Methods

Herein, 16 genes were identified as cASDEGs by intersecting the AS-related DEGs and cGAS–STING-related genes, with 15 genes being upregulated (Fig. 3D,E, **Supplementary Table 10**). LASSO (Fig. 4A,B) and RF (Fig. 4C,D) algorithms each revealed eight genes as critical cASDEGs, and SVM analysis identified 15 genes (Fig. 4E,F). Cross-validation among the three methods revealed four critical cASDEGs, namely *CSK*, *FABP5*, *BAG2*, and *GLA* (Fig. 4G, **Supplementary Table 11**).

External Validation of the Diagnostic Value of Critical cASDEGs and GSEA

The diagnostic potential of the four critical cASDEGs was validated both internally and externally using three datasets, namely GSE100927, GSE28829, and GSE43292. Notably, all four genes exhibited good diagnostic value (AUC value >0.75; Fig. 4H). Subsequently, the constructed nomogram model based on the four cASDEGs (Fig. 4I) was evaluated for its predictive efficiency using calibration curves and decision curve analysis in the training set and

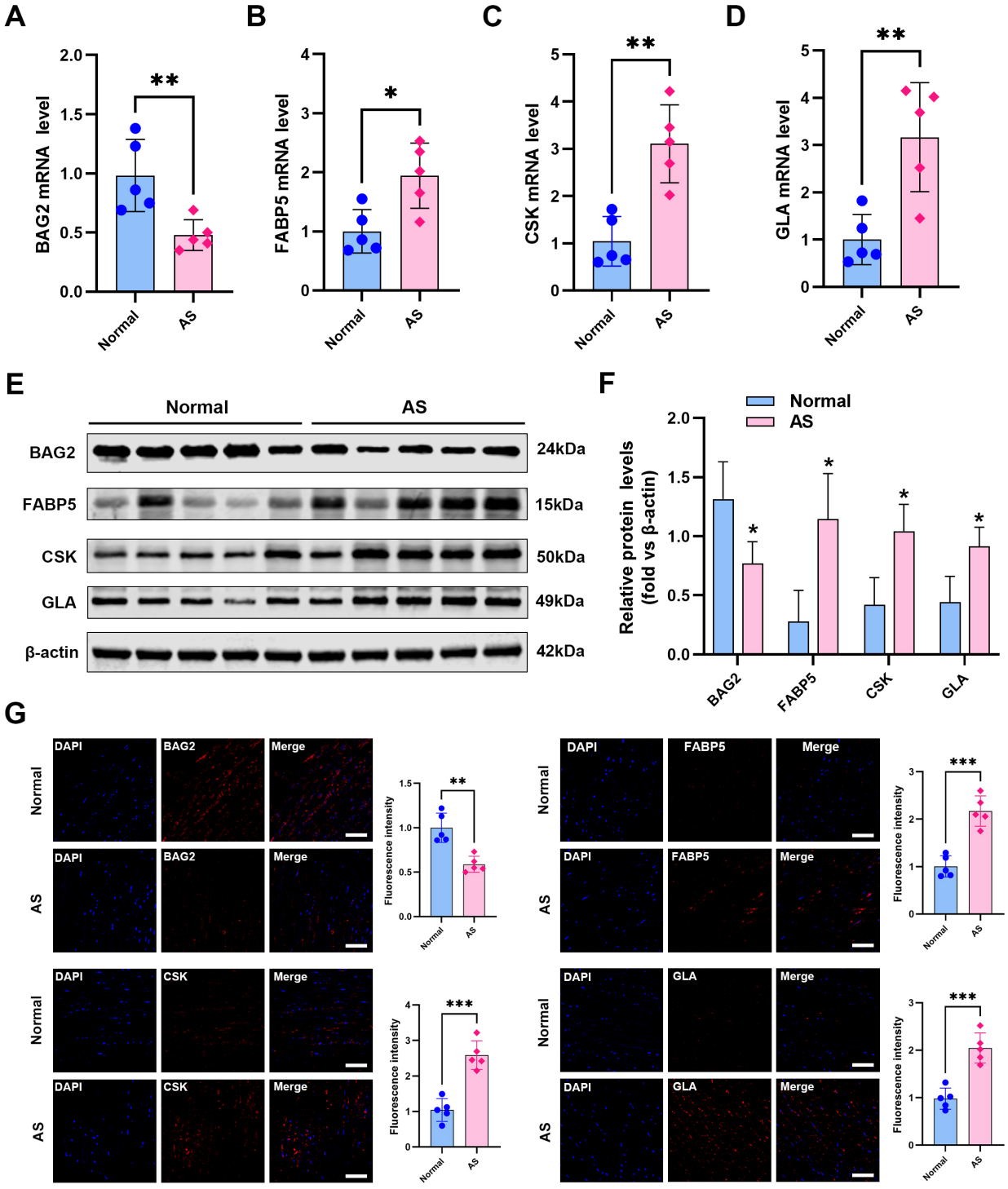

Fig. 6. Confirmation of the four core cASDEGs in human arterial tissues. (A–D) The relative expressions of the mRNA through RT-qPCR. (E,F) Representative Western blotting and quantitative analysis of the protein levels. (G) Representative immunofluorescence images of BAG2, CSK, FABP5, and GLA expression in normal and AS groups. Scale bar = 200 μm. *$p < 0.05$, **$p < 0.01$, ***$p < 0.001$ (the Normal group *vs.* the AS group). Abbreviations: AS, Arteriosclerosis; cASDEGs, cGAS–STING-related and AS-related differentially expressed genes; RT-qPCR, reverse transcription quantitative polymerase chain reaction.

validation set (Fig. 4J, **Supplementary Fig. 2A–D**). The nomogram demonstrated strong diagnostic performance. Through comprehensive GSEA, we systematically examined pathway enrichment disparities between patient subgroups stratified by expression levels of disease-associated genes. Our findings revealed that, within the disease cohort, the low expression of *BAG2*, coupled with the high expression of *FABP5* and *GLA* genes, correlated signifi-

cantly with the cytokine-cytokine receptor interaction pathway. Moreover, the low expression of *BAG2*, as well as the high expression of *CSK* and *GLA* genes, pertained to the nucleotide-binding oligomerization domain (NOD) -like receptor signaling pathway (**Supplementary Fig. 3A–H**, **Supplementary Tables 12–15**). These observations suggest that the modulation of these disease-critical genes may precipitate alterations in vascular function, trigger immune system activation, and modulate immune cell interactions. In parallel, the high expression of *BAG2*, along with the low expression of *CSK*, *FAPB5*, and *GLA* genes, was linked to the vascular smooth muscle cell contraction, focal adhesion, and TGF-β signaling pathways (**Supplementary Fig. 3A–H**, **Supplementary Tables 12–15**). These pathways are pivotal in the pathogenesis of the disease, indicating that the identified gene expression changes may play a critical role in disease progression by influencing these specific phenotypic outcomes.

Immune Infiltration in AS and the Relationship Between the Critical cASDEGs and Immune Cells

Inflammatory response and immune regulation play crucial roles in the pathogenesis of AS [24]. Immune infiltration analysis using the GSE100927 dataset was conducted to evaluate the involvement of various immune cells in the AS immune microenvironment (**Supplementary Table 16**). Comparative immune profiling revealed statistically significant variations in nine distinct immune cell populations between AS patients and healthy controls (Fig. 5A,B). These included: naïve and memory B cell subsets, antibody-secreting plasma cells, quiescent $CD4^+$ memory T cells, circulating monocytes, macrophage subtypes (M0 and M1), along with resting and activated mast cell populations. Additionally, the four cASDEGs were correlated with distinct patterns of immune cell infiltration (Fig. 5C). Specifically, *GLA*, *FABP5*, and *CSK* exhibited a positive correlation with M0 macrophages and follicular T helper (Th) cells, whereas *BAG2* was negatively correlated with these immune cells. Additionally, *GLA*, *FABP5*, and *CSK* exhibited a negative correlation with M1 macrophages and resting mast cells. Finally, the expression of these genes was assessed in clinical samples. Consistent with previous results, *BAG2* expression in AS decreased significantly, whereas that of *FABP5*, *CSK*, and *GLA* increased significantly ($p < 0.05$, Fig. 6A–G).

Discussion

In this study, three AS microarray datasets (namely GSE28829, GSE43292, and GSE100927) were utilized to identify four critical AS-related genes involved in the cGAS–STING pathway. The findings of this study provide valuable insights into the mechanisms of AS and the development of novel strategies for targeted treatment of AS via the cGAS–STING pathway.

Although abnormal activation of the cGAS–STING pathway has been reported in AS, to the best of our knowledge, its role in AS, especially its relationship with the complex oxidative stress and immune microenvironment in AS, has not been systematically explored. The abnormal release of mtDNA serves as a damage-associated molecular pattern and initiates downstream signaling pathways by activating the classical pattern recognition receptor cGAS [25]. The cGAS–STING pathway has been reported to be involved in various disease processes such as viral infections, tumor immunity, and aging [26–28]; however, most studies have focused on immune cells including dendritic cells, T lymphocytes, and natural killer cells. Notably, abnormal activation of the cGAS–STING pathway in non-immune cells can mediate disease development. For example, lipopolysaccharides can induce mtDNA release in endothelial cells, activating the cGAS–STING pathway to regulate cell proliferation and affect angiogenesis [29].

GLA, an enzyme involved in lipid metabolism, has been associated with cGAS–STING pathway regulation [30]. Reportedly, GLA deficiency leads to lipid accumulation in lysosomes, thereby activating the cGAS–STING pathway. This highlights the role of GLA in maintaining lysosomal homeostasis and preventing aberrant activation of the cGAS–STING pathway. FABP5 has been linked to the regulation of inflammation and immune responses [31], and it may indirectly affect cGAS–STING pathway-associated gene expression and immune response by modulating the nuclear factor kappa B (NF-κB) activity [32]. CSK, a tyrosine kinase, negatively regulates immune cell activation [33]. Reportedly, CSK inhibits the activity of Src family kinases, which can activate the cGAS–STING pathway; hence, CSK may have an inhibitory effect on the cGAS–STING pathway-mediated immune response [34]. Furthermore, our immune infiltration analysis revealed a positive correlation between the expression of *GLA*, *FABP5*, and *CSK* with M0 macrophages, and a negative correlation with M1 macrophages. While these associations are intriguing, we acknowledge that they are correlative in nature and do not imply direct regulatory effects. Nonetheless, they may reflect underlying biological relationships that warrant further investigation. Macrophages play central roles in the inflammatory response and atherosclerotic plaque progression [35], with M0 macrophages acting as precursors capable of phagocytosing lipids and debris, while M1 macrophages engage in pro-inflammatory cytokine production and tissue damage [36]. Therefore, the observed gene-immune cell associations may provide clues into how these genes are involved in shaping the immune landscape of AS, though causal relationships remain to be experimentally validated.

BAG2, a member of the BAG family of proteins, negatively regulates the NF-κB activity, which is a key regulator of the cGAS–STING pathway [37]. BAG proteins exhibit diverse functions in protein quality control, cell sig-

naling, apoptosis, and stress responses, which have been extensively studied in the context of cancer and neurodegenerative diseases [38]. However, the understanding of the specific role of BAG2 in immune modulation remains elusive. The negative correlation between BAG2 and immune cells may be associated with its regulatory effects on key immune pathways, which indirectly regulates the expression of immune cell markers, leading to the observed negative correlation. For instance, BAG2 can interact with and modulate the activity of immune signaling-related proteins, such as Th1 and Th2 cell differentiation [39].

Targeting the cGAS–STING pathway and its associated genes could offer a novel approach to modulating the immune response in AS patients, potentially halting or slowing disease progression. For example, *FABP5* has been shown to regulate lipid metabolism and inflammatory responses [40], both of which are crucial in AS pathogenesis. Similarly, CSK plays a key role in immune cell signaling [34], while BAG2 and GLA are involved in cellular stress responses and metabolic processes, respectively. These genes, therefore, represent potential molecular targets for the development of innovative treatments aimed at addressing the underlying immune dysregulation in AS. In addition to identifying potential therapeutic targets, our study also contributes to the broader understanding of the relationship between immune cell infiltration and AS. Our immune cell infiltration analysis revealed that the expression levels of the critical cASDEGs were closely associated with various immune cell types, further supporting the notion that immune dysregulation is a key driver of AS pathogenesis. These findings provide a foundation for future research on investigating the cGAS–STING pathway's role in modulating immune responses in AS, as well as the potential therapeutic interventions aimed at correcting immune imbalances.

Overall, GLA, a lysosomal enzyme involved in glycosphingolipid metabolism, may contribute to lysosomal dysfunction when downregulated or overexpressed, leading to mitochondrial damage and cytoplasmic leakage of mtDNA—a key trigger of cGAS activation. FABP5, known for its role in lipid transport and inflammatory regulation, may enhance NF-κB signaling, thereby indirectly amplifying cGAS–STING-mediated cytokine production and immune activation. Interestingly, although CSK is classically recognized as a negative regulator of Src family kinases, our findings showed that its expression was significantly upregulated in AS tissues. This elevation may reflect a compensatory response to heightened immune signaling or, under sustained inflammatory stress, could paradoxically promote STING activation via altered interactions with downstream adaptor proteins. Meanwhile, BAG2, a co-chaperone protein known to suppress NF-κB signaling and cellular stress responses, was significantly downregulated, potentially relieving inhibition on inflammatory pathways and contributing to sustained immune activation. Collectively, these genes may converge on the cGAS–STING axis through different but complementary mechanisms—affecting mitochondrial integrity, lipid metabolism, and immune signaling—thereby promoting chronic vascular inflammation and immune cell infiltration characteristic of advanced AS. This conceptual model provides a basis for future functional validation studies and highlights potential targets for therapeutic intervention.

Despite the insights gained, this study has several important limitations that should be acknowledged. First, our analyses relied heavily on publicly available Gene Expression Omnibus (GEO) datasets, which may introduce bias due to sample heterogeneity, batch effects, and inconsistencies in study design. Second, the validation experiments (RT-qPCR, Western blotting, and immunofluorescence) were conducted on only five clinical samples. This limited sample size, caused primarily by the difficulty in acquiring matched arteriosclerotic and non-arteriosclerotic arterial tissues, may reduce the statistical power and limit the generalizability of our findings. However, the consistency between the experimental validation results and the bioinformatics predictions lends support to the robustness of our observations. Third, while our immune cell infiltration analysis identified associations between the expression of key genes (e.g., *CSK*, *FABP5*, *GLA*, *BAG2*) and specific immune cell types (such as M0 and M1 macrophages), these findings are based on computational deconvolution and reflect correlative—not causal—relationships. Therefore, interpretations regarding macrophage polarization or immune modulation should be viewed with caution, and further *in vitro* or *in vivo* functional studies will be necessary to validate these associations mechanistically. Finally, while some of these limitations were mentioned briefly, we now present them more explicitly to ensure a balanced interpretation of our findings. Future studies involving larger patient cohorts, additional multi-omics data, and functional assays (e.g., gene knockout, overexpression, or co-culture models) are warranted to clarify the precise molecular roles of the identified genes in modulating the cGAS–STING pathway and their impact on the immune microenvironment in AS.

Conclusion

In summary, the findings of this study revealed that AS-related genes, namely *BAG2*, *GLA*, *FABP5*, and *CSK*, are all involved with the cGAS–STING pathway, either directly or indirectly, suggesting their potential roles in regulating immune responses and inflammatory processes in AS. Additional studies are required to thoroughly decipher how these genes interact with the cGAS–STING pathway and their roles in immune-related diseases.

Abbreviations

AS, Arteriosclerosis; cGAS, Cyclic guanosine monophosphate–adenosine monophosphate synthase; ML, machine learning; cASDEGs, cGAS–STING related and AS-related differentially genes; DEGs, differentially expressed genes; GEO, Gene Expression Omnibus; WGCNA, weighted gene co-expression network analysis; GO, Gene Ontology; KEGG, Kyoto Encyclopedia of Genes and Genomes; LASSO, Least Absolute Shrinkage and Selection Operator; SVM, support vector machine; RF, random forest; CSK, C-src tyrosine kinase; FABP5, fatty acid binding protein 5; BAG2, B-cell lymphoma 2-associated athanogene; GLA, alpha-galactosidase A.

Availability of Data and Materials

The datasets (GSE28829, GSE43292, and GSE100927) generated and analyzed during the current study are available in the GEO dataset repository (https://www.ncbi.nlm.nih.gov/gds).

Author Contributions

The study's conception was performed by FZ and GXW. Material preparation and analysis were performed by FZZ, LCY, YXC and DX. The first draft of the manuscript was written by FZZ and LCY. All authors have been involved in revising it critically for important intellectual content. All authors give final approval of the version to be published. All authors have participated sufficiently in the work to take public responsibility for appropriate portions of the content and agreed to be accountable for all aspects of the work in ensuring that questions related to its accuracy or integrity.

Ethics Approval and Consent to Participate

This study was conducted in adherence to the tenets of the Declaration of Helsinki. All methods were performed in accordance with the relevant guidelines and regulations. The studies involving humans were approved by the Ethics Committee of Fujian Provincial Hospital (license number: K2021-04-042). All subjects have written informed consent.

Acknowledgment

Not applicable.

Funding

The study was supported by the Natural Science Foundation of Fujian Province (Grant No.2021J05066).

Conflict of Interest

The authors declare no conflict of interest.

Supplementary Material

Supplementary material associated with this article can be found, in the online version, at https://doi.org/10.24976/Discov.Med.202537199.133.

References

[1] Jurgens CY, Lee CS, Aycock DM, Masterson Creber R, Denfeld QE, DeVon HA, *et al*. State of the Science: The Relevance of Symptoms in Cardiovascular Disease and Research: A Scientific Statement From the American Heart Association. Circulation. 2022; 146: e173–e184. https://doi.org/10.1161/CIR.0000000000001089.

[2] Goldsborough E, 3rd, Osuji N, Blaha MJ. Assessment of Cardiovascular Disease Risk: A 2022 Update. Endocrinology and Metabolism Clinics of North America. 2022; 51: 483–509. https://doi.org/10.1016/j.ecl.2022.02.005.

[3] Nayor M, Brown KJ, Vasan RS. The Molecular Basis of Predicting Atherosclerotic Cardiovascular Disease Risk. Circulation Research. 2021; 128: 287–303. https://doi.org/10.1161/CIRCRESAHA.120.315890.

[4] Kong P, Cui ZY, Huang XF, Zhang DD, Guo RJ, Han M. Inflammation and atherosclerosis: signaling pathways and therapeutic intervention. Signal Transduction and Targeted Therapy. 2022; 7: 131. https://doi.org/10.1038/s41392-022-00955-7.

[5] Luca AC, David SG, David AG, Țarcă V, Pădureț IA, Mîndru DE, *et al*. Atherosclerosis from Newborn to Adult-Epidemiology, Pathological Aspects, and Risk Factors. Life (Basel, Switzerland). 2023; 13: 2056. https://doi.org/10.3390/life13102056.

[6] Pickett JR, Wu Y, Zacchi LF, Ta HT. Targeting endothelial vascular cell adhesion molecule-1 in atherosclerosis: drug discovery and development of vascular cell adhesion molecule-1-directed novel therapeutics. Cardiovascular Research. 2023; 119: 2278–2293. https://doi.org/10.1093/cvr/cvad130.

[7] Wu X, Zhang H, Qi W, Zhang Y, Li J, Li Z, *et al*. Nicotine promotes atherosclerosis via ROS-NLRP3-mediated endothelial cell pyroptosis. Cell Death & Disease. 2018; 9: 171. https://doi.org/10.1038/s41419-017-0257-3.

[8] Batty M, Bennett MR, Yu E. The Role of Oxidative Stress in Atherosclerosis. Cells. 2022; 11: 3843. https://doi.org/10.3390/cells11233843.

[9] Sun L, Wu J, Du F, Chen X, Chen ZJ. Cyclic GMP-AMP synthase is a cytosolic DNA sensor that activates the type I interferon pathway. Science (New York, N.Y.). 2013; 339: 786–791. https://doi.org/10.1126/science.1232458.

[10] Cohen D, Melamed S, Millman A, Shulman G, Oppenheimer-Shaanan Y, Kacen A, *et al*. Cyclic GMP-AMP signalling protects bacteria against viral infection. Nature. 2019; 574: 691–695. https://doi.org/10.1038/s41586-019-1605-5.

[11] Hopfner KP, Hornung V. Molecular mechanisms and cellular functions of cGAS-STING signalling. Nature Reviews. Molecular Cell Biology. 2020; 21: 501–521. https://doi.org/10.1038/s41580-020-0244-x.

[12] Huang LS, Hong Z, Wu W, Xiong S, Zhong M, Gao X, *et al*. mtDNA Activates cGAS Signaling and Suppresses the YAP-Mediated Endothelial Cell Proliferation Program to Promote Inflammatory Injury. Immunity. 2020; 52: 475–486.e5. https://doi.org/10.1016/j.immuni.2020.02.002.

[13] Chakraborty A, Li Y, Zhang C, Li Y, Rebello KR, Li S, *et al*. Epigenetic Induction of Smooth Muscle Cell Phenotypic Alterations in Aortic Aneurysms and Dissections. Circulation. 2023; 148: 959–977. https://doi.org/10.1161/CIRCULATIONAHA.123.063332.

[14] Barrett T, Wilhite SE, Ledoux P, Evangelista C, Kim IF, Tomashevsky M, *et al*. NCBI GEO: archive for functional genomics data sets–update. Nucleic Acids Research. 2013; 41: D991–5. https://doi.org/10.1093/nar/gks1193.

[15] Wickham H, Chang W, Henry L, Pedersen TL, Takahashi K, Wilke CO, *et al*. Create Elegant Data Visualisations Using the Grammar of Graphics [R package ggplot2 version 3.3.2]. 2020. https://doi.org/10.32614/cran.package.ggplot2.

[16] Langfelder P, Horvath S. WGCNA: an R package for weighted correlation network analysis. BMC Bioinformatics. 2008; 9: 559. https://doi.org/10.1186/1471-2105-9-559.

[17] Yu G, Wang LG, Han Y, He QY. clusterProfiler: an R package for comparing biological themes among gene clusters. Omics: a Journal of Integrative Biology. 2012; 16: 284–287. https://doi.org/10.1089/omi.2011.0118.

[18] Friedman J, Hastie T, Tibshirani R. Regularization Paths for Generalized Linear Models via Coordinate Descent. Journal of Statistical Software. 2010; 33: 1–22.

[19] Meyer D, Dimitriadou E, Hornik K, Weingessel A, Leisch F. Misc Functions of the Department of Statistics (e1071), TU Wien. R package. 2008; 1: 5–24.

[20] Kuhn M. Building Predictive Models in R Using the caret Package. Journal of Statistical Software. 2008; 28: 1–26. https://doi.org/10.18637/jss.v028.i05.

[21] Liaw A, Wiener MC. Classification and Regression by randomForest. R News. 2002; 2: 18–22.

[22] Wang S, Liu H, Yang P, Wang Z, Ye P, Xia J, *et al*. A role of inflammaging in aortic aneurysm: new insights from bioinformatics analysis. Frontiers in Immunology. 2023; 14: 1260688. https://doi.org/10.3389/fimmu.2023.1260688.

[23] Newman AM, Liu CL, Green MR, Gentles AJ, Feng W, Xu Y, *et al*. Robust enumeration of cell subsets from tissue expression profiles. Nature Methods. 2015; 12: 453–457. https://doi.org/10.1038/nmeth.3337.

[24] Xie W, Chen S, Luo H, Kong C, Wang D. Critical gene signature and immunological characterization in peripheral vascular atherosclerosis: novel insights from mendelian randomization and transcriptomics. Frontiers in Genetics. 2024; 15: 1361445. https://doi.org/10.3389/fgene.2024.1361445.

[25] Liu Z, Wang M, Wang X, Bu Q, Wang Q, Su W, *et al*. XBP1 deficiency promotes hepatocyte pyroptosis by impairing mitophagy to activate mtDNA-cGAS-STING signaling in macrophages during acute liver injury. Redox Biology. 2022; 52: 102305. https://doi.org/10.1016/j.redox.2022.102305.

[26] Decout A, Katz JD, Venkatraman S, Ablasser A. The cGAS-STING pathway as a therapeutic target in inflammatory diseases. Nature Reviews. Immunology. 2021; 21: 548–569. https://doi.org/10.1038/s41577-021-00524-z.

[27] Samson N, Ablasser A. The cGAS-STING pathway and cancer. Nature Cancer. 2022; 3: 1452–1463. https://doi.org/10.1038/s43018-022-00468-w.

[28] Paul BD, Snyder SH, Bohr VA. Signaling by cGAS-STING in Neurodegeneration, Neuroinflammation, and Aging. Trends in Neurosciences. 2021; 44: 83–96. https://doi.org/10.1016/j.tins.2020.10.008.

[29] Wu B, Xu MM, Fan C, Feng CL, Lu QK, Lu HM, *et al*. STING inhibitor ameliorates LPS-induced ALI by preventing vascular endothelial cells-mediated immune cells chemotaxis and adhesion. Acta Pharmacologica Sinica. 2022; 43: 2055–2066. https://doi.org/10.1038/s41401-021-00813-2.

[30] Wang A, Chen C, Mei C, Liu S, Xiang C, Fang W, *et al*. Innate immune sensing of lysosomal dysfunction drives multiple lysosomal storage disorders. Nature Cell Biology. 2024; 26: 219–234. https://doi.org/10.1038/s41556-023-01339-x.

[31] Guo Y, Liu Y, Zhao S, Xu W, Li Y, Zhao P, *et al*. Oxidative stress-induced FABP5 S-glutathionylation protects against acute lung injury by suppressing inflammation in macrophages. Nature Communications. 2021; 12: 7094. https://doi.org/10.1038/s41467-021-27428-9.

[32] Field CS, Baixauli F, Kyle RL, Puleston DJ, Cameron AM, Sanin DE, *et al*. Mitochondrial Integrity Regulated by Lipid Metabolism Is a Cell-Intrinsic Checkpoint for Treg Suppressive Function. Cell Metabolism. 2020; 31: 422–437.e5. https://doi.org/10.1016/j.cmet.2019.11.021.

[33] Zhu S, Wang H, Ranjan K, Zhang D. Regulation, targets and functions of CSK. Frontiers in Cell and Developmental Biology. 2023; 11: 1206539. https://doi.org/10.3389/fcell.2023.1206539.

[34] Gao P, Hu MM, Shu HB. CSK promotes innate immune response to DNA virus by phosphorylating MITA. Biochemical and Biophysical Research Communications. 2020; 526: 199–205. https://doi.org/10.1016/j.bbrc.2020.03.069.

[35] Mills CD. M1 and M2 Macrophages: Oracles of Health and Disease. Critical Reviews in Immunology. 2012; 32: 463–488. https://doi.org/10.1615/critrevimmunol.v32.i6.10.

[36] Lv JJ, Wang H, Zhang C, Zhang TJ, Wei HL, Liu ZK, *et al*. CD147 Sparks Atherosclerosis by Driving M1 Phenotype and Impairing Efferocytosis. Circulation Research. 2024; 134: 165–185. https://doi.org/10.1161/CIRCRESAHA.123.323223.

[37] Qin L, Guo J, Zheng Q, Zhang H. BAG2 structure, function and involvement in disease. Cellular & Molecular Biology Letters. 2016; 21: 18. https://doi.org/10.1186/s11658-016-0020-2.

[38] Huang X, Shi D, Zou X, Wu X, Huang S, Kong L, *et al*. BAG2 drives chemoresistance of breast cancer by exacerbating mutant p53 aggregate. Theranostics. 2023; 13: 339–354. https://doi.org/10.7150/thno.78492.

[39] Li C, Shi H. BAG2 Is a Novel Prognostic Biomarker and Promising Immunotherapy Target in Uveal Melanoma. Critical Reviews in Eukaryotic Gene Expression. 2023; 33: 55–71. https://doi.org/10.1615/CritRevEukaryotGeneExpr.2023048565.

[40] Seo J, Jeong DW, Park JW, Lee KW, Fukuda J, Chun YS. Fatty-acid-induced FABP5/HIF-1 reprograms lipid metabolism and enhances the proliferation of liver cancer cells. Communications Biology. 2020; 3: 638. https://doi.org/10.1038/s42003-020-01367-5.